Int. J. Electrochem. Sci., 14 **(2019)** 6759 – 6772, doi: 10.20964/2019.07.28

International Journal of
ELECTROCHEMICAL
SCIENCE
www.electrochemsci.org

Corrosion inhibition effect of 2-Hydroxy Phosphonoacetic Acid and Pyrophosfate on Q235 steel, Electrochemical Noise and EIS analysis

Chenxi Yi[1,2,*] *Benfeng Zhu*[1]

[1] Department of Chemistry, Zhejiang University, Hangzhou, Zhejiang 310027, China
[2] Bureau of Inno & Entre Town, Hangzhou Economic & technological development area, Hangzhou, Zhejiang 310000, China
[*]E-mail: yichenxi2013@163.com

Received: 27 February 2019 / *Accepted:* 27 April 2019 / *Published:* 10 June 2019

The inhibiting behavior of $K_4P_2O_7$, $C_2H_5O_6P$ and their mixture on Q235 steel corroding in the simulated stratum water has been investigated by using electrochemical noise (EN) and electrochemical impedance spectroscopy (EIS) techniques. The results show that the physical adsorption of KPP onto Q235 surface at 60 °C is somewhat faster than the chemisorption of HPAA. In the re-plotted energy distribution plot, the difference of the region where the EN energy is mostly accumulated may be adopted to distinguish the chemisorption and physical adsorption of inhibitors. Finally, the variation tendency of the charge transfer resistance obtained by EIS technique is just opposite to that of fractal dimension obtained by EN technique, which may hint that the initial corrosion processes of metals can be in-situ monitored by using EN technique expediently.

Keywords: Q235 steel; corrosion; inhibiting behavior; EIS; EN.

1. INTRODUCTION

Mild steel such as Q235 has been widely used in petroleum, chemical and engineering industries[1]. However, it can be easily destroyed during their serving processes, especially in highly aggressive environments, such as the stratum water of high chloride concentration[2-6].

One of the practical and effective methods to prevent corrosion is the utilization of inhibitors. Generally, it is assumed that the first stage in the inhibiting process is the adsorption of the inhibitors onto the metal surface. The adsorption processes of inhibitors are influenced by the nature and surface charge of the metals, and the chemical structure of the inhibitor[7]. Physical adsorption and chemisorption are the principal or basic types of interaction between inhibitor and metal surface. The organic molecules adsorb on the metal surface though heteroatom, such as nitrogen, oxygen, sulfur and

phosphorus, whose electrons have a π character[8, 9]. Generally, chemisorption is specific for certain metals and not completely reversible, which involves the electron transfer therefore depends on both the metal and inhibitor.

Nowadays, electrochemical noise (EN) technique has widely been applied to monitor the onset of the transient events, such as pitting, stress corrosion or cracking corrosion[10-16]. The prime attraction of EN technique is its high sensitivity to the corrosion process, which often causes unexpected and rapid damage and is hard to be predicted with traditional techniques (weight loss, polarization tests, electrochemical impedance spectroscopy)[17-20]. Unfortunately, few literatures have reported the correlation between EN features and the inhibitor adsorption mechanism[21]. On the other hand, fractal dimension (D_f) has also been widely used for different purpose, especially to quantitatively analyze the fractal objects to characterize their surface roughness, which then provide additional valuable information about the properties and dynamics of the investigated systems[22-26]. However, also few literatures have adopted D_f to study the protection processes of inhibitors onto metals[14].

Tahe oil field is an important oil field of China, which stratum water simultaneously contains extreme high concentrations of the water-soluble Ca^{2+} (0.08M) and Cl^- (3.0M) ions. Although the addition of some phosphate inhibitors can result in the formation of the insolubly highly crystalline Ca-phosphate salts onto the surface of the used Q235 steel[27, 28], the pitting corrosion of Q235 is still serious[28].

In the present paper, EN and EIS (electrochemical impedance spectroscopy) techniques are adopted to study the protective behavior of inhibitors $K_4P_2O_7$ (KPP), $C_2H_5O_6P$ (HPAA) and their mixture on Q235 steel, which is corroding in the simulated stratum water. The main purpose of this work is to probe into the relationship between the inhibitor adsorption behavior and the EN features, which is generated during the corrosion processes of Q235 steels.

2. EXPERIMENTAL

The simulated stratum water of Tahe oil field, which contains 3.0M NaCl and 0.08M $CaCl_2$, was prepared using analytical grade reagents and used as the corrosive solutions. The pH value of the solutions was adjusted to 4.00 by using the diluted HCl. Potassium pyrophosphate ($K_4P_2O_7$ or KPP) and 2-Hydroxyphosphonoacetic acid ($C_2H_5O_6P$ or 50% HPAA) were purchased from Aladdin Industrial Co. Ltd. (China) and Taihe Water Treatment Technologies Co. Ltd. (China), and used as received and without further treatment.

Weight loss measurements of Q235, which is corroding in the simulated stratum water (denoted as "solutions" hereinafter) containing HPAA and KPP of different mass ratio, was performed according to standard ISO 8407:2009, IDT. Briefly, inhibitor of calculated concentration was first added into a beaker, which contains 1 L simulated stratum water, then the beaker was put into a water bath to maintain the specific temperature. The Q235 steel coupons with the dimensions of 50mm×25mm×2mm were sectioned from the Q235 plate, which was also received from Taihe Water

Treatment Technologies Co. Ltd. (China). The average corrosion rate during the investigated time period was calculated using eq. 1.

$$r_{corr} = \frac{8.76\times10^4\cdot\Delta m}{S\cdot t\cdot\rho} \qquad \textbf{eq. 1}$$

where r_{corr} is the average corrosion rate; Δm is the mass loss of Q235 steel (g); S is the surface area of the plate (cm^2); ρ is the density of Q235 steel (equal to 7.85 $g\cdot cm^{-3}$); t is the test time (h), unless other stated, t=48 h is chosen in this article; the conversion factor 8.76×10^4 is used to translate the corrosion rate into the unit ($mm\cdot y^{-1}$). The accurate weight was obtained by analytical balance (AL104 METTLER TOLEDO).

The electrochemical potential noise, which was generated during the corrosion process of Q235 steel in the simulated stratum water of different inhibitor at open circuit potential, was recorded with PARSTAT 2273 (Princeton Applied Research) at a sampling rate of 4 Hz. Cylindrical Q235 steel with an exposed area of 0.50 cm^2 was sealed with Teflon and used as working electrode. Prior to each measurement, the working surface was abraded and polished to mirror, washed with double-distilled water, rinsed with acetone, and finally dried with N_2. A large area platinum foil and a saturated calomel electrode (SCE) were used as auxiliary and reference, respectively. The interval sample time was 0.25 second, by which most usual corrosion processes can be detected. The frequency window of the observation can be calculated roughly[29].

$$\left(C_1^l, C_2^l\right) = (2^l\Delta t, 2^{l-1}\Delta t) \qquad \text{eq. 2}$$

where l is the number of the crystal, and Δt is the sampling interval of 0.25 s. During the EN measurements, the experimental device was shielded in a Faradaic cage. The EN measurements were performed in a quiescent solution at 60±1 °C without stirring, which was also controlled by a thermostatically water bath.

Hurst index of the measured EN data series is calculated by using the so-called the R/S technique, which was proposed by Hurst[30] and used by Mandelbrot and Wallis[31].

$$R_{(t,S)}\Big/S_{(t,S)} \propto S^H \qquad \text{eq. 3}$$

where R(t, S) stands for the difference between the maximum and minimum values of the variable, S(t, S) for the square root of the sample sequential variance, and the Hurst exponent (H) varies between 0<H<1. Then, the (local) fractal dimension (D_f) is derived by using the following eq. 4 [32, 33].

$$D_f = 2 - H \qquad \text{eq. 4}$$

EIS tests were also carried out with PARSTAT 2273 impedance measurement apparatus at the rest potential, the applied sinusoidal voltage amplitude was 5 mV and the sweep always initiated from the frequency of 100 kHz to 0.01 Hz.

3. RESULTS AND DISCUSSION

3.1 Thermodynamic absorption mechanism

The surface coverage degree (θ, in some lectures, θ equals to inhibition efficiency η) of inhibitor on steel could be obtained:

$$\theta = \eta = \frac{\Delta m_0 - \Delta m_1}{\Delta m_0} \qquad \text{eq. 5}$$

where Δm_1 and Δm_0 are the mass loss with or without the inhibitor (HPAA and KPP). Figure 1 shows the relationship between the singular inhibitor concentration (c) and the surface coverage. For both HPAA and KPP, the plot of θ against ln$c$ gives a straight line, which is the characteristics of Temkin adsorption isotherm given by[34, 35]:

$$\exp(-2\alpha\theta) = \mathrm{K}c \qquad \text{eq. 6}$$

where α is the molecular interaction parameter, K is the equilibrium constant of the adsorption process which is related to the standard free energy ΔG^0_{ads} of the adsorption process:

$$\mathrm{K} = \frac{1}{55.5}\exp(-\frac{\Delta G^0_{ads}}{RT}) \qquad \text{eq. 7}$$

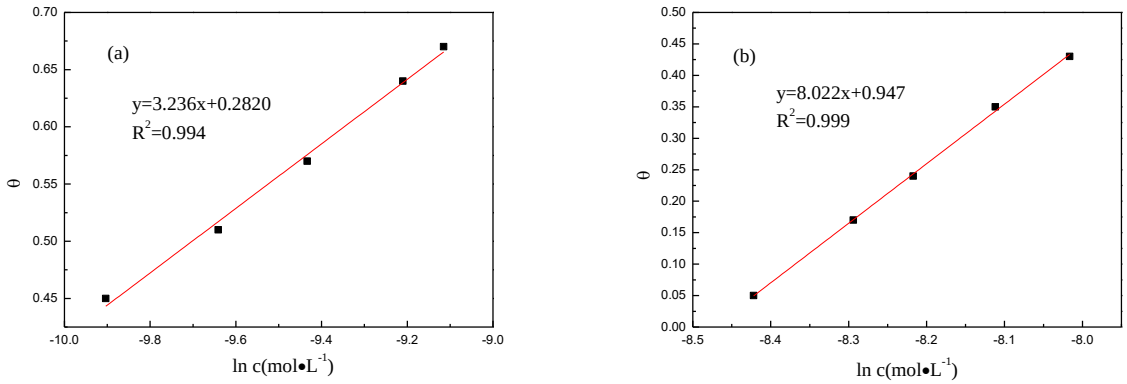

Figure 1. The relationship between θ and **ln*c*** for HPAA (a) and KPP (b) at 60 ºC

Generally, ΔG^0_{ads} of -40 KJ·mol^{-1} is widely adopted as a critical point to differentiate the adsorption types, ΔG^0_{ads} of more negative value than -40 KJ·mol^{-1} indicates the charge sharing or transfer from inhibitor molecules to metal, i.e. chemisorption[36, 37]. ΔG^0_{ads} calculated from eq. 8 equals to -44.16 KJ·mol^{-1} and -35.56 KJ·mol^{-1} for HPAA and KPP, respectively, which therefore indicates that HPAA mainly chemically adsorbed on Q235 surface at 60 ºC, whereas KPP mainly physically adsorbed.

Table 1. Corrosion rate and inhibition efficiency for blended inhibitor in simulation stratum water, obtained by weight loss measurement (60 ºC, t=48h)

Item	r_{corr}/mm·y^{-1}	η/%
Blank	0.0979	--
80 mg·L^{-1} KPP +20 mg·L^{-1} HPAA	0.0329	66.19
70 mg·L^{-1} KPP +30 mg·L^{-1} HPAA	0.0214	77.95
60 mg·L^{-1} KPP +40 mg·L^{-1} HPAA	0.0079	91.91
50 mg·L^{-1} KPP +50 mg·L^{-1} HPAA	0.0207	78.68
40 mg·L^{-1} KPP +60 mg·L^{-1} HPAA	0.0428	55.90
30 mg·L^{-1} KPP +70 mg·L^{-1} HPAA	0.0579	40.46

For the reason that both HPAA and KPP exhibit low η values on Q235 surface (less than 70%) in the investigated dosage region (Figure 1), their blended mixture of different ratio is intentionally

used to elevate their inhibition efficiency (Table 2). It can be seen that η increases conspicuously after employing their blended mixture, whilst the mixture containing 60 mg·L^{-1} KPP and 40 mg·L^{-1} HPAA is the highest. Therefore, such mixture is designated as the blended inhibitor and adopted in the following studies.

Figure 2 shows the FTIR spectra of Q235 surfaces after their immersion in the simulated stratum water of 100 mg·L^{-1} different inhibitors (HPAA, KPP and blended inhibitor) for 90 min. The 1100 cm^{-1} band is the dominant feature of the spectra which is assigned to P-O^{-} groups; bands in the region 736-774 cm^{-1} correspond to symmetric stretching of the P-O-P group, and the 870-900 cm^{-1} bands are assigned to the asymmetric stretching mode of P-O-P linkages[38, 39]. Whilst, several broad and small bands in the region of 2500-2950 cm^{-1} are assigned to the hydrogen phosphonate, H-OPO$_2$C, moieties[40]; characteristic P-OH band appears at 2327 cm^{-1}, and O-H stretching vibration bands has also been detected above 3600 cm^{-1}. These characteristics undoubtedly show the existence of the so-called "synergistic effect" between KPP and HPAA. Moreover, some weak jagged bands have detected in the region 1500-2500 cm^{-1} and 3500-3700 cm^{-1} by using HPAA, and the bands at 1265 (P=O) and 1030 cm^{-1} (P-O-Fe) attribute to the iron phosphate, which suggest the chemisorption of microscale HPAA onto steel surface.

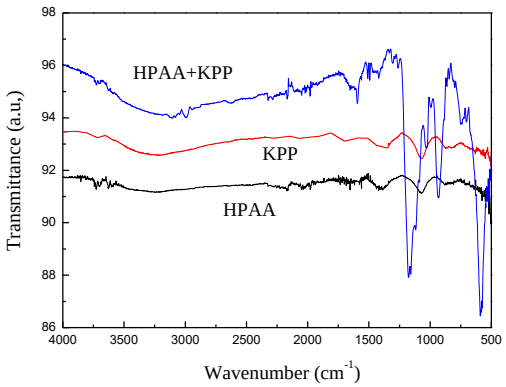

Figure 2. FTIR spectra of Q235 steel surfaces after their immersion in the simulated stratum water of 100 mg·L^{-1} different inhibitors for 90 min, 60 ºC

3.2 Electrochemical measurements

Electrochemical noise (EN) technique has been carried out to qualitatively analyze the relationship between the EN features and the corrosion process. Fast wavelet transformation (FWT) technique of the fourth order (db4)[41] is applied to obtain the so-called energy distribution plot (EDP) by using following general relations[42]:

$$E_j^D = \sum_{k=1}^{N/2^j} D_{j,k}^2, (j = 1,2, \dots, J) \quad \text{eq. 9}$$

$$E_J^S = \sum_{k=1}^{N/2^j} S_{J,k}^2, (j = 1,2, \dots, J) \quad \text{eq. 10}$$

$$E_N = \sum_{j=1}^{J} E_j^D + E_J^S \quad \text{eq. 11}$$

where D_1, $D_2 \dots D_J$ and S_J are designated as the so-called "crystals", E_j and E_J are the energies accumulated at crystals D_J and S_J, respectively. Then, RP-EDP plot was further obtained by re-plotting

the resulted EDP plot via discounting the energy contribution of S_8 crystal from the ensemble signal energy, videlicet, removing the energy contribution of "D_c trend".

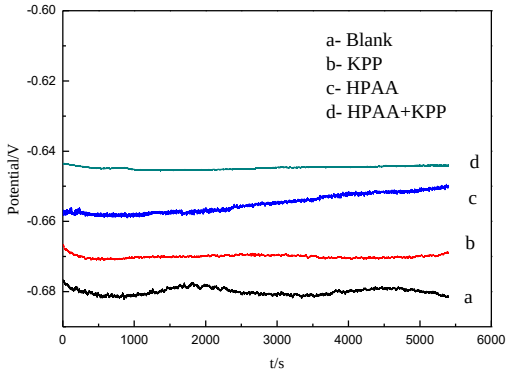

Figure 3. Time-domain potential EN for Q235 steel corroding in the simulated stratum water containing different inhibitor within the initial 90 min at 60 ºC

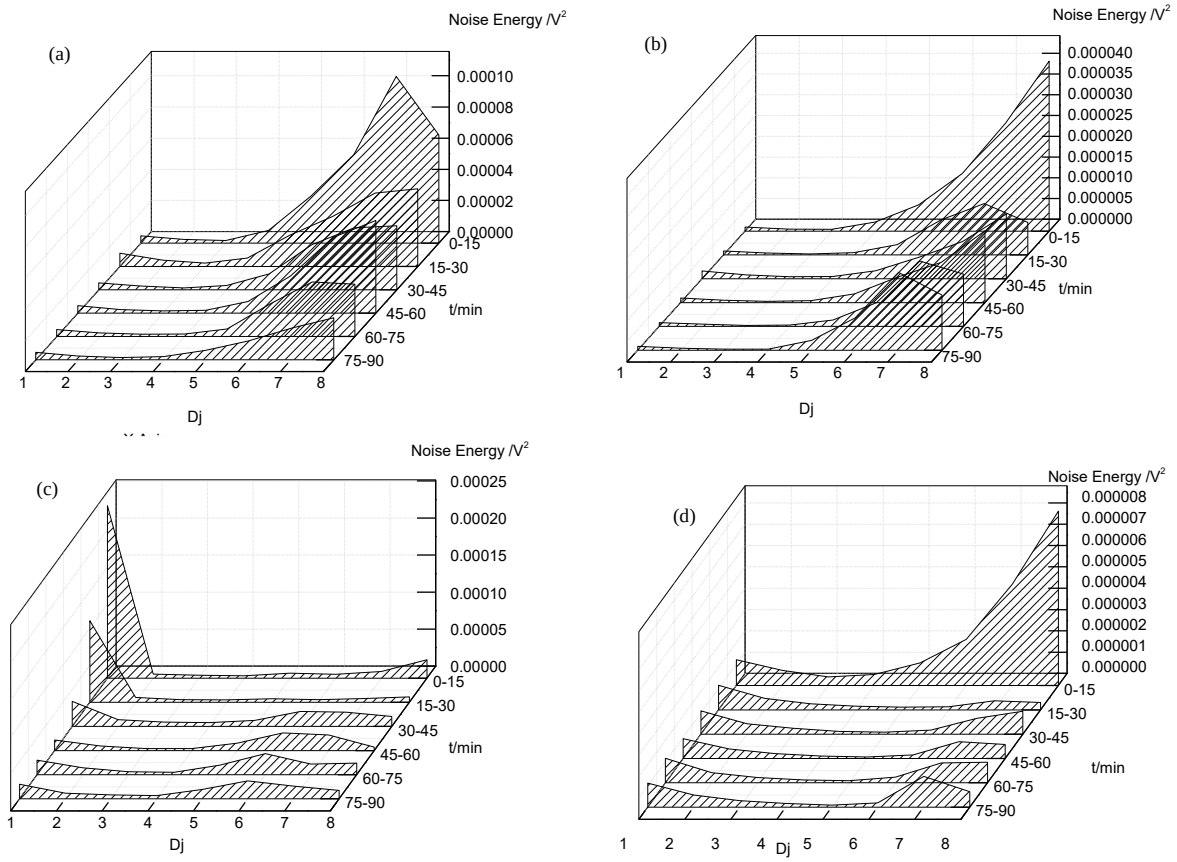

Figure 4. RP-EDP plots for Q235 corroding in the solutions containing different inhibitor at 60 ºC: (a) blank; (b) KPP; (c) HPAA; (d) blended inhibitor.

Generally, EN is composed of distinct type of events that can be distinguished by their different time constant, and the initiation and growth of pit embryo always occurs prior to the other types of localized corrosion and is also much faster than diffusion of aggressive ions and desorption of corrosion products[11]. According to our previous studies and other literatures[41, 43, 44], the RP-

EDP can be divided into three segments: (1) region I between D_1 and D_3 mainly characterizes the nucleation process; (2) region II between D_4 and D_6 mainly characterizes the growth process; (3) region III between D_6 and D_8 mainly reflects the information about the diffusion process.

Figures 3-4 shows the time-domain potential EN of Q235 steel corroding in the simulated stratum water containing different inhibitor within the initial 90 min at 60 ºC, and their corresponding RP-EDP plots, respectively. In the cases of no inhibitor (Figure 4a) and only individual KPP inhibitor (Figure 4b), the energy accumulates predominantly in the coarse crystals (D_6-D_8), which indicates that the nucleation and growth of pits on Q235 surface is fast and rapid, and the corrosion rate is limited by the diffusion process, i.e., the cathodic reagents move to the active corroding points[4, 42]. Whilst, Figure 4b also shows that the protection effect caused only by KPP is quite limited.

For the individual HPAA inhibitor system (Figure 4c) and with the prolongation of immersion time, the EN energy deposited in region III decreases, whereas the energy accumulated in region I increases, especially, the EN energy for Q235 corroding in HPAA system is much larger than those in KPP (Figure 4b) and blank (no inhibitor, Figure 4a) systems. These phenomena seemingly indicate that the corroding rate of Q235 in HPAA contained solution is much larger than those in KPP or no inhibitor contained solutions.

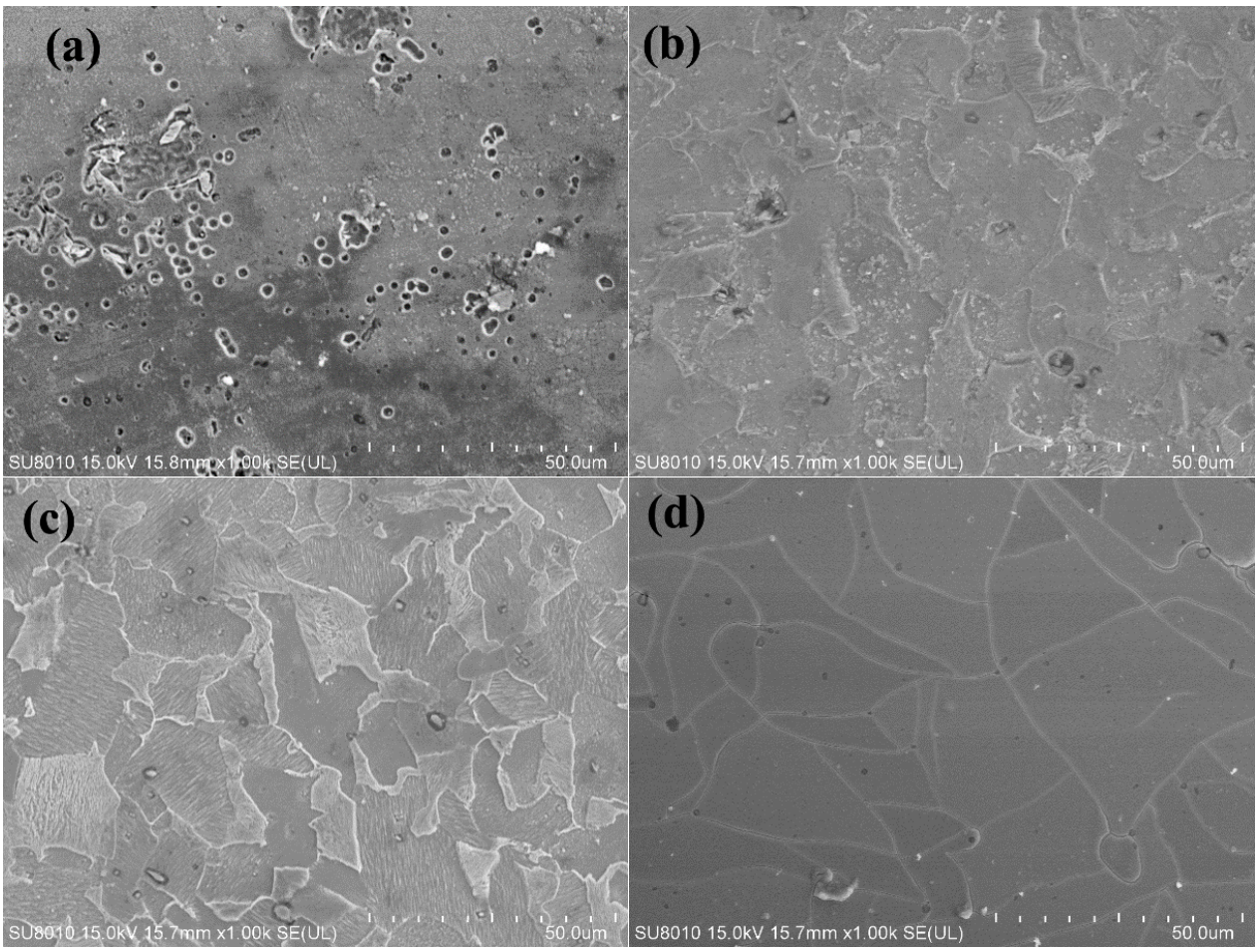

Figure 5. SEM image of Q235 steel after corroding in the simulation stratum water of different inhibitor for 90 min. (a) Blank; (b) KPP; (c) HPAA; (d) Blended inhibitor

Therefore, weight loss and SEM are adopted to characterize the corrosion severity of Q235 in the solutions containing different inhibitors. Figure 5 shows the morphologies of Q235 after corroded in these different solutions for 90 min. It can be clearly seen that both the number and the diameter of the already formed pits increase with the change of corrosive solutions from no inhibitor (Figure 5a) through single KPP (Figure 5b) and single HPAA (Figure 5c) to the blended inhibitor (Figure 5d), and the weight loss also shows that the inhibition efficiency (60 ºC, t=48h) of KPP (15%) is smaller than that of HPAA (64%), both of which undoubtedly indicate that Q235 suffers the most serious pitting corrosion. Then, why the EN energy for Q235 corroding in HPAA system is the highest?

The main difference for HPAA and KPP adsorption onto Q235 surface is that, HPAA mainly chemically adsorbed on Q235 surface at 60 ºC, whereas KPP mainly physically adsorbed (Section 3.1). The formation of chemical bonds (such as P-O-Fe) should cause the charge transfer between Q235 and HPAA, these charge transfers between inhibitors and metals can also be detected by EN technique[17]. Moreover, many chemical reactions have also been investigated by using EN technique[45, 46]. Therefore, the highest EN energy for Q235 corroding in HPAA system (Figure 4) should be caused by the chemical bond formation between Q235 and HPAA. On the other hand, a period of time is necessary for HPAA to achieve its adsorption equilibrium onto Q235 surface, and this adsorption process is always coupled with the formation of the chemical bonds to form a layer of protectively integrated molecular film. The gradual completion of this film therefore results in that, the film growth and the local diffusion of inhibitor molecules (from other place such as the bulk solution to the growth sites or film defects) gradually controls the film formation process. This kind of local diffusion may be much similar to that observed in metal deposition process[41]. Therefore, with the prolongation of immersion time, the EN energy accumulated in region I decreases, whilst those defined in regions II and III increase, and at last, a kind of dynamic equilibrium between corrosion and chemisorption gradually establishes (Figure 4c).

When Q235 is corroding in the solutions containing the blended inhibitor (60 $mg \cdot L^{-1}$ KPP +40 $mg \cdot L^{-1}$ HPAA), the EN energy mainly accumulates in regions I and III (Figure 4d). During the initial immersion period (~15 min), the EN energy deposited in region III is the highest, which should be attributed to the fast adsorption of inhibitors, especially the physical adsorption of KPP on Q235, which causes the prominent diffusion effect. However, the bonding reactions of HPAA with Fe should compete the active sites (the practical electrode substrate surfaces usually possess many imperfections such as plateau edges, kinks, vacancies and emergent screw dislocations[47]) with KPP to form a layer of protectively integrated molecular film on Q235 surface. Because the chemisorption is more irreversible than the physical adsorption, the growth of the chemically formed film certainly gradually consumes the active sites on Q235 surface and therefore decreases the local diffusion effect of inhibitors, which results in the decrease of the EN energy deposited in region III. From Figure 4d, it can also be seen that the chemisorption of HPAA begins to play a dominant role after Q235 is immersed in the blended inhibitor contained solutions for 15 min, and also a kind of dynamic equilibrium between corrosion and chemisorption gradually establishes (Figure 4d). Although the transformation tendencies of RP-EDP shapes, especially the ordinate values are much different (Figure 4), which may be attributed to the “synergistic effect” of KPP and HPAA and waits for further deep

exploring, the difference in the RP-EDP region, where the EN energy is mostly accumulated, may be adopted to distinguish the chemisorption and physical adsorption of inhibitors.

Finally, it should be mentioned that the adsorption process of KPP and HPAA is always coupled with the corrosion of Q235 steel, the EN energy should be simultaneously attributed to both of them, even if their contribution fraction to the total EN energy are much different during the different immersion period.

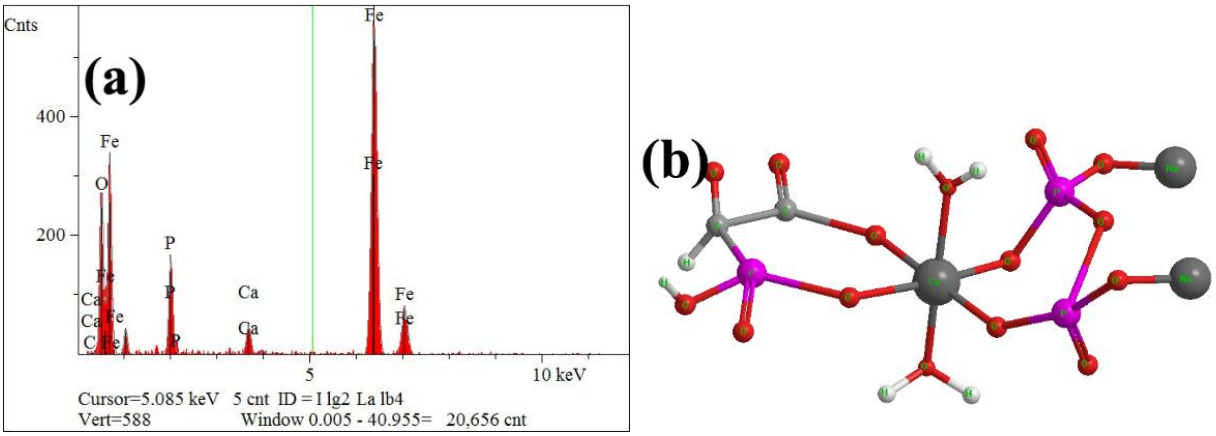

Figure 6. (a) The EDS element distribution and (b) the supposed element structure of protected film, after Q235 steel immersed in the simulation stratum water containing blended inhibitor for 90 min, 60 ºC

Figure 5 shows that the blended inhibitor gives excellent protection to Q235 steel against chloride corrosion, therefore, EDS and XPS technique are adopted to further characterize the film composition formed in the solutions containing the blended inhibitor.

Figure 6a reveals that calcium (in solutions) has involved into the surface deposited film, and the atom number ratio of the film is P:Ca:Na:C:O=3:1:2:2:14, approximately. Based on the reported researches[39, 48-50], the surface film formed by the blended inhibitor may possess the structure schematically presented in

Figure 6b: the calcium in central is 6-coordinate, which is surrounded by two chelating phosphorous compounds, forming six-membered rings: Ca-O-P-C-C-O-Ca and Ca-O-P-O-P-O-Ca.

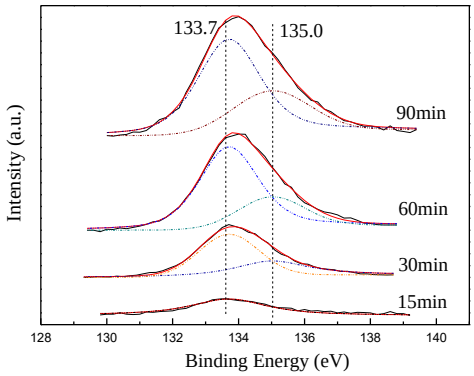

Figure 7. XPS P 2p spectra of Q235 steel after corroded in the solutions containing the blended inhibitor for different time (60 °C)

Figure 7 shows the XPS P2p spectra of Q235 steel after it being corroded in the solutions containing the blended inhibitor for different time. The typical P2p peak can be consistently fitted by two nearly Gaussian, which suggests two mixtures are involved in the surface film: pyrophosphate group and 2-hydroxylphosphonoacetic group from KPP and HPAA, centered at 133.7eV, 135.0eV, respectively[51, 52]. The two Gaussian peak value increase with the prolongation of immersion time, which suggests the incrassation of the anticorrosion film or the nucleation/growth of the inhibitor layer on Q235 surface, and therefore the good inhibition efficiency of the blended inhibitor. Furthermore, the peak of 135.0eV (for HPAA) at 15min is absent or can be neglected, which implies that the physical adsorption of KPP is somewhat faster than the chemisorption of HPAA, and may also support the result shown in Figure 4d that the EN energy accumulated in region III is the largest during the initial 15min corrosion period.

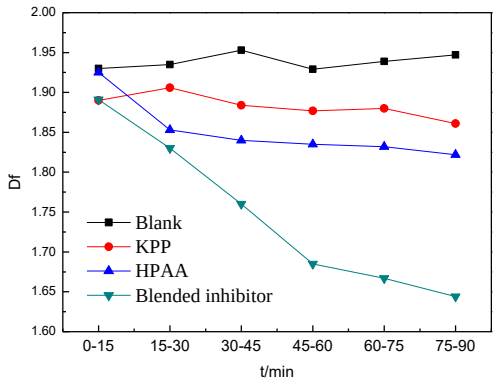

Figure 8. Fractal dimension of Q235 steel corroding in the solutions containing different inhibitors (60 °C)

D_f of Q235 steel during it being corroding in the solutions of different inhibitors is also calculated by using eq.3 (Figure 8). It can be seen that the D_f value of no inhibitor always possesses the highest value, which indicates the largest roughness or corrosion sensitivity[22]. After corroding for 90 min, D_f of Q235 steel ranks as no inhibitor > KPP > HPAA > blended inhibitor, which agrees well with the corrosion sensitivity obtained by SEM (Figure 5) and weight loss.

The corrosion processes of Q235 in the solutions of different inhibitors are also investigated using EIS technique, and only one capacitive arc in the middle-high frequency region is observed (Figure 9). With the help of both the features of the EIS diagrams (such as the number and the width of the phase angle peak of the peak in Bode plots and the number of the capacitance loops in Nyquist plots) and the method developed by Weijde[53, 54]. Simultaneously, only time-constant of the EIS plots can be determined. Therefore, the equivalent electrical circuit (EEC) shown as an insert in Figure 9 has been adopted to fit these EIS plots by Z-view software.

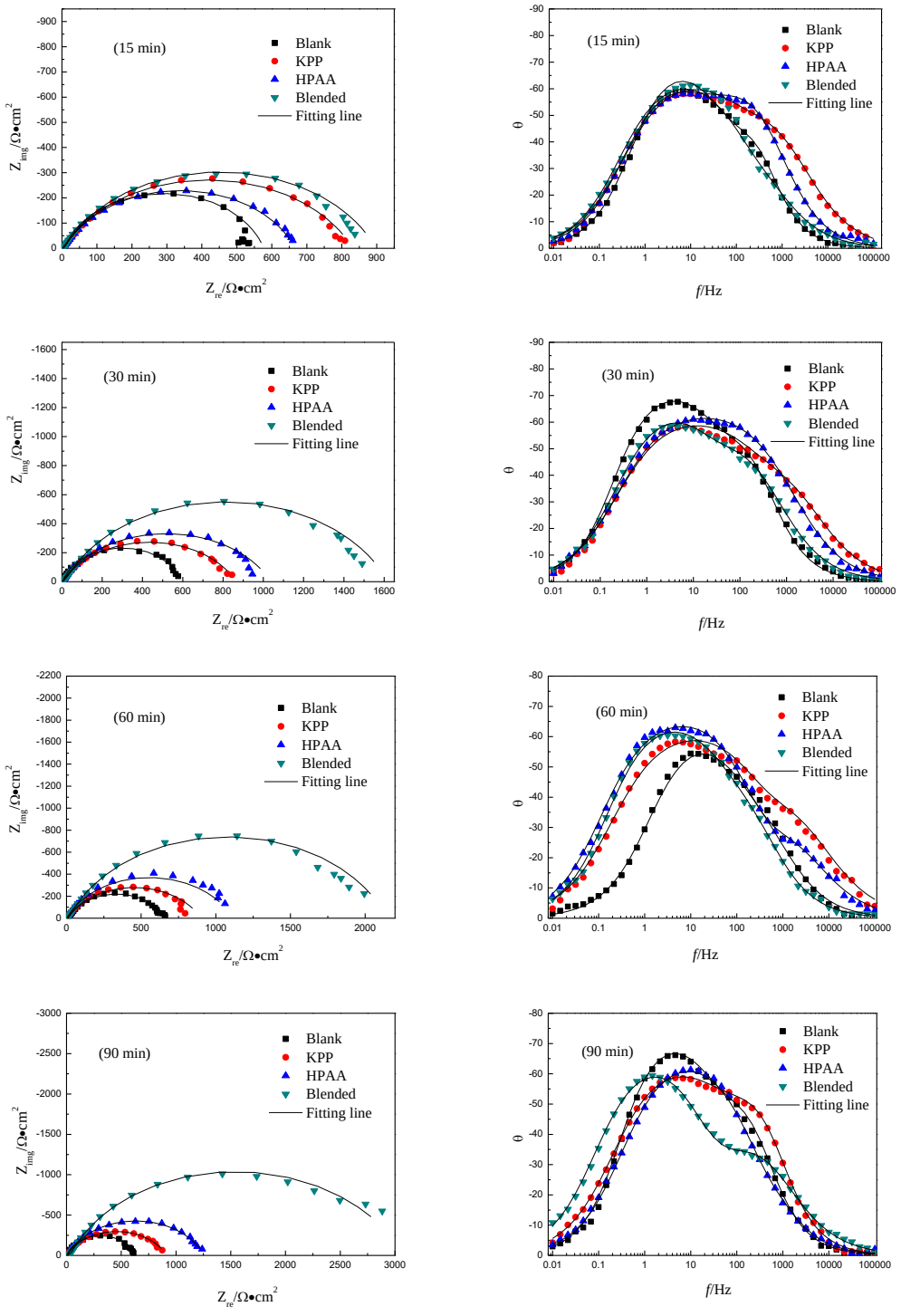

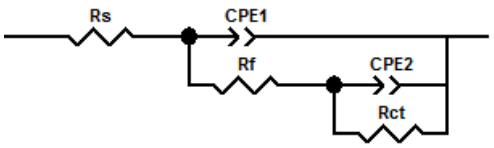

Figure 9. EIS spectra of Q235 steel corroding in the solutions containing different inhibitors at selected immersion time, and the EEC models proposed to fit the EIS data

Generally, the charge transfer resistance (Rct) is widely used to characterize the corrosion rate, and the larger the charge transfer resistance the lower the corrosion rate[55]. Therefore, Rct is extracted and plotted versus the corrosion time (Figure 10). It can be seen that Rct of Q235 steel (corroding in the solutions containing different inhibitors) ranks as no inhibitor < KPP < HPAA < blended inhibitor, which also agrees well with the corrosion sensitivity obtained by SEM (Figure 5) and weight loss. Moreover, when simultaneously inspect Figure 8 and Figure 10, it is interesting to find that the variation tendency of Rct is just opposite to that of D_f, which may hint that the initial corrosion processes of metals can be expediently in-situ monitored by using EN techniques.

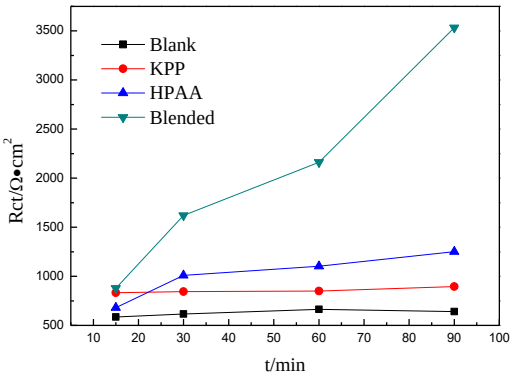

Figure 10. Relationship of R_{ct} ($\Omega \cdot cm^2$) versus time for Q235 steel corroding in the solutions containing different inhibitors at 60 ºC

4. CONCLUSION

The corrosion behavior of Q235 steel in the simulated stratum water (high concentration chloride medium) containing different inhibitor (KPP, HPAA and their mixture) has been investigated. HPAA and KPP are mainly chemically and physically adsorbed onto Q235 surface at 60 °C, respectively, and the physical adsorption of KPP is somewhat faster than the chemisorption of HPAA. In the investigated conditions and when the mixture of KPP and HPAA are added as inhibitors into the corrosive solutions, the chemisorption of HPAA begins to play a dominantly protective role after Q235 is corroded for 15 min.

The difference in the RP-EDP region, where the EN energy is mostly accumulated, may be adopted to distinguish the chemisorption and physical adsorption of inhibitors. At last, the variation tendency of Rct obtained by EIS technique is just opposite to that of D_f obtained by EN technique,

which may hint that the initial corrosion processes of metals can be in-situ monitored by using EN technique expediently.

ACKNOWLEDGEMENT
This work was supported by the National Natural Science Foundation of China (Project 51771173, 21273199, 51131005)

References

1. B.W. Allcock and P.A. Lavin, *Surf. Coat. Tech.*, 163-164 (2003) 62.
2. K.Y. Ann and H.-W. Song, *Corros. Sci.*, 49 (2007) 4113.
3. Y. Wang, G. Cheng, W. Wu, Q. Qiao, Y. Li and X. Li, *Appl. Surf. Sci.*, 349 (2015) 746.
4. N. Dai, J. Zhang, Q. Chen, B. Yi, F. Cao and J. Zhang, *Corros. Sci.*, 99 (2015) 295.
5. M. Criado, I. Sobrados, J. Sanz and J. M. Bastidas, *Surf. Coat. Tech.*, 258 (2014) 485.
6. F. Ansari, R. Naderi and C. Dehghanian, *RSC Adv.*, 5 (2015) 706.
7. H.J. Guadalupe, E. Garcia-Ochoa, P. Maldonado-Rivas, J. Cruz and T. Pandiyan, *J. Electroanal. Chem.*, 655 (2011) 164.
8. M. Awad, F. Mahgoub and M. El-Iskandarani, *J. Mol. Struc.-Theochem*, 531 (2000) 105.
9. M.K. Awad, *J. Electroanal. Chem.*, 567 (2004) 219.
10. Z.-n. Yang, Z. Zhang, W.-h. Leng, K. Ling and J.-q. Zhang, *Trans. Nonferrous Met. Soc. China*, 16 (2006) 209.
11. F.H. Cao, Z. Zhang, J.X. Su, Y.Y. Shi and J.Q. Zhang, *Electrochimi. Acta*, 51 (2006) 1359.
12. U. Bertocci and F. Huet, *Corrosion*, 51 (1995) 131.
13. U. Bertocci and J. Kruger, *Surf. Sci.*, 101 (1980) 608.
14. E. García-Ochoa and J. Genesca, *Surf. Coat. Tech.*, 184 (2004) 322.
15. A. Conde and J. de Damborenea, *Surf. Coat. Tech.*, 150 (2002) 212.
16. S.Y. Arman, R. Naderi and B.P. Markhali, *RSC Adv.*, 4 (2014) 39045.
17. Y. Chen, Z.N. Yang, Y.W. Liu, H.H. Zhang, J.Y. Yin, Y. Xie and Z. Zhang, *J. Taiwan Inst. Chem. E.*, 80 (2017) 908.
18. B. Ramezanzadeh, S.Y. Arman, M. Mehdipour and B.P. Markhali, *Appl. Surf. Sci.*, 289 (2014) 129.
19. Z. Quan, P.-Q. Wu, L. Tang and J.P. Celis, *Appl. Surf. Sci.*, 253 (2006) 1194.
20. G. Gusmano, G. Montesperelli, M. Rapone, G. Padeletti, A. Cusmà, S. Kaciulis, A. Mezzi and R. D. Maggio, *Surf. Coat. Tech.*, 201 (2007) 5822.
21. B.P. Markhali, R. Naderi, M. Mahdavian, M. Sayebani and S.Y. Arman, *Corros. Sci.*, 75 (2013) 269.
22. L.-j. Zhang, X.-b. Zhu, Z. Zhang and J.-q. Zhang, *Trans. Nonferrous Met. Soc. China*, 19 (2009) 496.
23. G.A. McRae, M.A. Maguire, C.A. Jeffrey, D.A. Guzonas and C.A. Brown, *Appl. Surf. Sci.*, 191 (2002) 94.
24. P.R. Roberge, *J. Appl. Electrochem.*, 23 (1993) 1223.
25. M.G. Mahjani, R. Moshrefi, A. Sharifi-Viand, A. Taherzad, M. Jafarian, F. Hasanlou and M. Hosseini, *Chaos Soliton. Fract.*, 91 (2016) 598.
26. E. Sarmiento, J.G. González-Rodriguez and J. Uruchurtu, *Surf. Coat. Tech.*, 203 (2008) 46.
27. K.D. Demadis, M. Papadaki, R.G. Raptis and H. Zhao, *Chem. Mater.*, 20 (2008) 4835.
28. R.M. Colodrero, A. Cabeza, P. Olivera-Pastor, M. Papadaki, J. Rius, D. Choquesillo-Lazarte, J.M. García-Ruiz, K.D. Demadis and M.A. Aranda, Cryst. *Growth. Des.*, 11 (2011) 1713.
29. Z. Dong, X. Guo, J. Zheng and L. Xu, *Electrochem. Commun.*, 3 (2001) 561.
30. H.E. Hurst, *P. I. Civil. Eng.*, 5 (1956) 519.
31. B.B. Mandelbrot and J.R. Wallis, *Water Resour. Res.*, 5 (1969) 321.
32. E. García-Ochoa and F. Corvo, *Electrochem. Commun.*, 12 (2010) 826.

33. S. Kulesza and M. Bramowicz, *Appl. Surf. Sci.*, 293 (2014) 196.
34. A. Frumkin, *Z. Phys.*, 116 (1925) 466.
35. S. Bilgic and M. Şahin, *Mater. Chem. Phys.*, 70 (2001) 290.
36. E. Khamis, F. Bellucci, R. Latanision and E. El-Ashry, *Corrosion*, 47 (1991) 677.
37. F.M. Donahue and K. Nobe, *J. Electrochem. Soc.*, 112 (1965) 886.
38. H. Liu, T. Chin and S. Yung, *Mater. Chem. Phys.*, 50 (1997) 1.
39. L.M. Grover, U. Gbureck, A.J. Wright and J.E. Barralet, *J. Am. Ceram. Soc.*, 88 (2005) 3096.
40. Y. Zhu, Z. Sun, Y. Zhao, J. Zhang, X. Lu, N. Zhang, L. Liu and F. Tong, *New J. Chem.*, 33 (2009) 119.
41. Z. Zhang, W.H. Leng, Q.Y. Cai, F.H. Cao and J.Q. Zhang, *J. Electroanal. Chem.*, 578 (2005) 357.
42. [42] Y. Shi, Z. Zhang, J. Su, F. Cao and J. Zhang, *Electrochimi. Acta*, 51 (2006) 4977.
43. D.H. Xia, S.Z. Song and Y. Behnamian, *Corros. Eng. Sci. Techn.*, 51 (2016) 527.
44. X. Huang, Y. Chen, T. Fu, Z. Zhang and J. Zhang, *J. Electrochem. Soc.*, 160 (2013) D530.
45. V.A. Tyagai, *Electrochimi. Acta*, 16 (1971) 1647.
46. C. Yi, X. Du, Y. Yang, Y. Chen, G. Wei, Z. Yang and Z. Zhang, *Int. J. Electrochem. Sc.*, 12 (2017) 3597.
47. M.C. Lefebvre and B.E. Conway, *J. Electroanal. Chem.*, 480 (2000) 46.
48. K.D. Demadis and S.D. Katarachia, *Phosphorus. Sulfue.*, 179 (2004) 627.
49. H. Assaaoudi, I.S. Butler and J.A. Kozinski, *Solid State Sci.*, 8 (2006) 1353.
50. F.N. Shi, J.C. Almeida, L.A. Helguero, M.H. Fernandes, J.C. Knowles and J.O. Rocha, *Inorg. Chem.*, 54 (2015) 9929.
51. X. Wang, J. Shi, Z. Li, S. Zhang, H. Wu, Z. Jiang, C. Yang and C. Tian, *ACS Appl. Mater. Inter.*, 6 (2014) 14522.
52. F. Li, H. Zhong, G. Zhao, S. Wang and G. Liu, *Appl. Surf. Sci.*, 353 (2015) 856.
53. D.H. van der Weijde, E.P.M. van Westing and J.H.W. de Wit, *Corros. Sci.*, 36 (1994) 643.
54. P. Campestrini, E.P.M. van Westing and J.H.W. de Wit, *Electrochimi. Acta*, 46 (2001) 2553.
55. F. Da-jing, M. Xu-hui, Z. Ye-ming, C. Zhi-liang, L. Min and G. Fu-xing, *Anti-Corros. Method. M.*, 56 (2009) 226.